2018-06-15

Tidal stream resource characterisation in progressive versus standing wave systems

Ward, SL

10.1016/j.apenergy.2018.03.059
Applied Energy

Tidal stream resource characterisation in progressive versus standing wave systems

Sophie L. Ward[a], Peter E. Robins[b*], Matt J. Lewis[a], Gregorio Iglesias[c], M Reza Hashemi[d], Simon P. Neill[b].

*Corresponding author: p.robins@bangor.ac.uk

[a]Centre for Applied Marine Sciences, Marine Centre Wales, Bangor University, Menai Bridge, LL59 5AB, UK.
[b]School of Ocean Sciences, Bangor University, Menai Bridge, LL59 5AB, UK.
[c]University of Plymouth, School of Marine Science and Engineering, Marine Building, Drake Circus, Plymouth PL4 8AA, UK.
[d]Department of Ocean Engineering and Graduate School of Oceanography, Rhode Island University, USA.

Abstract

Characterisations of the tidal stream resource and its variability over various timescales are crucial for the development of the tidal stream energy industry. To date, no research has compared resource sensitivity in standing wave (when peak currents occur midway between high and low water) and progressive wave (where peak currents occur at high and low water) tidal systems. Here, we compare the flow regimes of standing wave versus progressive wave systems and the associated variations in tidal stream power with applications to device deployment options (floating-platform turbines versus bottom-mounted turbines). We use a validated 3D numerical model (ROMS) of a globally-significant tidal energy shelf sea region (Irish Sea), to test the hypotheses that the influence on potential extractable energy, and suitability for different devices, may be markedly different between these contrasting systems. Power density was also calculated and compared for floating versus bottom-mounted devices using *in-situ* current data (ADCPs) obtained from a standing wave site and a progressive wave site. We show that progressive wave systems are characterised by velocity-asymmetry over a tidal cycle (i.e. stronger peak flows at high water than at low water), leading to power-asymmetry. Such power asymmetry was shown to have more of an effect on floating device technology, where an assumed turbine depth tracks the sea surface, in contrast to bottom-mounted technology, where the hub height is fixed at a certain position above the sea bed. Shallow, high-flow regions where tidal range is large contained up to 2.5% more power density from bottom-mounted compared with floating turbines; however, there were areas where floating devices were exposed to higher mean currents over a tidal cycle. Standing wave systems, where flow asymmetry is minimised, did not particularly favour either technology. The results highlight the requirement for detailed resource assessments to consider the vertical plane, and are applicable to all potential tidal stream energy sites.

Keywords: Tidal energy, Floating turbine, 3D modelling, resource characterisation, ROMS, ADCP, Irish Sea

1. Introduction

Exploiting the abundant potential global tidal energy resource could provide us with a renewable and largely predictable source of power that has the potential to reduce our reliance on fossil fuels, thus helping to meet global targets for renewables (Lewis et al. 2015). Shelf sea regions that exhibit large tidal ranges or strong tidal currents contain significant potential for tidal energy extraction, such as the northwest European shelf seas surrounding the United Kingdom (Flather 1976; Yates et al. 2013; Robins et al. 2015). Whereas tidal impoundments (lagoons or barrages) exploit the potential energy of the rising and falling tide, in-stream tidal turbines harness the kinetic energy of tidal currents. These resources can be predicted over long timescales using ocean models, which to some extent can capture hourly-to-decadal variability in current speeds and, hence, available power; however, the vertical variability of the resource within the water column is less well understood, because many tidal resource assessment models are based on depth-averaged 2D assumptions.

Considerable research, development and innovation (RD&I) into tidal stream energy technologies and resource characterisation are being conducted throughout the United Kingdom. The world's first fully-operational grid-connected tidal stream array (3 × 100 kW turbine array) has been deployed by Nova Innovation in Shetland, Scotland (www.novainnovation.com). In addition, phase 1A (4 x 1.5 MW turbine array) of the 400 MW MeyGen project in the Pentland Firth, Scotland, is completed and grid connected (www.atlantisresourcesltd.com). Both of these schemes have adopted bottom-mounted tidal stream devices, where the turbine hub height is located at a fixed distance above the sea bed.

Across Europe, there has been significant development of turbines deployed from floating platforms, advantages and disadvantages of which are outlined in Table 1. For these floating devices, the platform is usually tethered to the seabed to constrain horizontal movement, but is free to move vertically with changes in sea surface elevation. The turbine is mounted at a fixed depth relative to the platform, and so the hub height tracks the free surface, and consequently the turbine encounters a different flow regime over time than a fixed hub height turbine would at the same location (Fig. 1), particularly when the tidal range is large. Several prototype floating tidal stream energy devices have been designed and tested *in situ* (e.g. Wang et al. 2010), including Bluewater's BlueTEC device which was installed in the Wadden Sea (2015, www.bluewater.com), Oceanflow's Evopod (1/4 scale) demonstration at

Sanda Sound, Scotland (2014, www.oceanflowenergy.com), and Hydra Tidal's Morild II was deployed in 2010 for two years in the Lofoten Islands, Norway (hydratidal.wix.com).

Table 1. Advantages and disadvantages of floating tidal stream energy devices.

Advantages of floating-platform devices	***Disadvantages of floating-platform devices***
Can be deployed in strong near-surface flows and in deep water.	Larger potential (negative) influence of wave-current interactions near surface (than bottom-mounted devices)
Self-aligned with the flow direction - maximises energy generation.	Require more expensive flexible electrical cables than bottom-mounted devices.
Minimise device fatigue due to self-alignment with the flow and waves.	Bio-fouling and corrosion of platform, tethers, and moorings.
Cheaper and quicker installation than piling, smaller vessels needed for deployment.	Large strain on tethers and moorings.
Simplifies maintenance (compared to bottom-mounted devices)	

Despite the level of technological advancement of floating devices, there has been little consideration within resource assessments of the possible changes in energy yield that results from such technologies, compared with 'conventional' bottom-mounted devices. In particular, few studies have considered tidal stream resource variability over the vertical water column, other than the work of Sanchez et al. (2014a; 2014b) and Thiébaut and Sentchev (2017). Several recent resource assessment studies have looked beyond simply characterising the peak M_2 tidal flows and suitable water depths, to address: (i) resource variabilities at tidal timescales caused by coastal effects (e.g. Piano et al. 2017; O'Hara Murray and Gallego 2017); (ii) astronomical tidal variations generating daily-to-interannual resource variability (e.g. Robins et al. 2015; Guillou et al. 2018); and (iii) the effects of wave-current interactions on the resource (e.g. Hashemi et al. 2015a; Lewis et al. 2014).

Sanchez et al. (2014a) used 3D hydrodynamic model simulations to compare the potential annual power generation from floating (upper 65% of the water column) versus bottom-mounted devices (lower 65% of the water column), using the power curve of the Evopod floating device. They found that the annual electricity production in the estuary, the Ria de Ortigueira (Spain), increased by 40% using a floating device rather than a bottom-mounted device, because of higher velocities higher up the water column. Sanchez et al. (2014b) subsequently reported that the simulated impacts on estuarine circulation were comparable when energy was extracted by theoretical floating or bottom-mounted devices. A more recent study by Thiébaut

and Sentchev (2017) considered the tidal energy resource off the coast of Brittany, focussing on tidal asymmetry. Comparing vertical variations in observational flow data, Thiébaut and Sentchev (2017) estimated that the monthly mean technical resource was up to 50% greater in the upper half of the water column than in the lower half, again due to higher velocities in the upper half of the water column.

In this paper, we use models and observations to examine variability in the tidal stream resource over the vertical in relation to the phasing of surface elevations and tidal velocities that produce either standing or progressive wave systems. To our knowledge, prior to this work, no study has investigated the simulated differences in power density from floating and bottom-mounted devices when positioned at similar hub heights in these different flow regimes, which is an important consideration, particularly for relatively shallow tidal stream energy sites. The tidally-energetic Irish Sea is used here as a case study, but the principle findings highlight relevant considerations for potential tidal stream development sites across the globe.

2. Standing and progressive tidal waves

Where a tidal current is described as a *standing wave*[1] system, slack water coincides with high and low water, with peak flood and ebb flows occurring at mid-tide (Fig. 2a). Conversely, if peak tidal currents occur at high and low water, with slack water at mid-tide, then the tidal current is referred to as a *progressive wave* system (Fig. 2b). In a progressive wave system, the peak currents are more affected by water depth changes than for a standing wave system, with the potential for weaker peak currents at low water than at high water, because of the increased influence of sea bed friction compared with total water depth (Lewis et al. 2017). This effect will be more pronounced in shallow waters, and for larger tidal ranges. Conversely, the effect is reduced as the wave moves towards a standing wave system, because peak flood and ebb currents occur in similar water depths (i.e. around mean sea level, MSL). In reality, few locations are purely standing or progressive, but are more likely to be characterised as 'mixed' or partially-progressive wave systems.

Within shelf sea regions, there is often considerable variation in the nature of the tidal wave. As the ocean tide propagates onto shelf seas, tidal wave reflections within coastal basins, bays, and estuaries result in the formation of standing waves (Pugh 1996). Where the basin length aligns with the wavelength of tidal oscillations, resonance occurs and the tide is amplified, producing large tidal ranges, such as in the Bristol Channel, United Kingdom (Pugh 1996) and the Bay of Fundy, Canada (Garrett 1972). Tidal propagation through topographically complex regions such as island archipelagos can generate large pressure gradient forces that can influence the

[1] Where 'tides' are characterised as shallow water 'waves'.

nature of the tidal wave – changing from standing to progressive within a few kilometres (e.g. Winant and Gutiérrez de Velasco 2003; Waldman et al. 2017). Long channels or estuaries (relative to the tidal length scale) experience progressive wave systems towards their head because of a significant damping effect of bottom friction that delays the flow relative to the elevation (Li and O'Donnell 2005).

Here, we develop an ocean model for the Irish Sea (described in Sections 2 and 3). We simulate 3D tidal current velocities in relation to the phasing of the surface elevations and, hence, characterise the tidal regime (standing through to progressive) throughout the Irish Sea. By simulating current speeds likely encountered by both bottom-mounted and floating tidal energy devices, we then calculate the expected differences in power density between the two schemes, under realistic conditions within the Irish Sea. We extend this analysis to data from two ADCPs, obtained from contrasting standing vs progressive wave systems in the Irish Sea. These results are presented in Section 4, followed by our Discussions (Section 5) and Conclusions (Section 6).

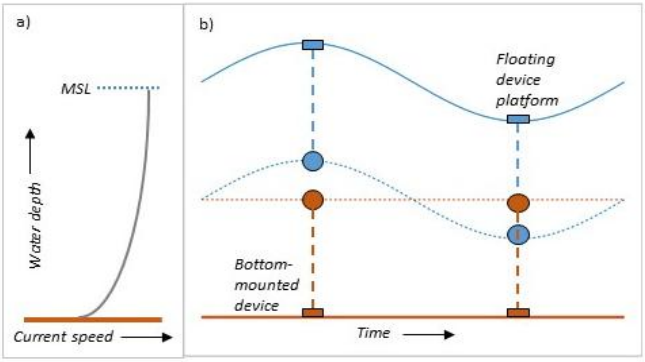

Figure 1: (a) Schematic of a typical vertical current velocity profile. (b) Schematic showing different configurations of floating-platform (blue) and bottom-mounted (red) turbines in the water column. The hub height of the floating turbine varies with sea surface height, hence potentially experiencing a greater range of velocities than the bottom-mounted turbine.

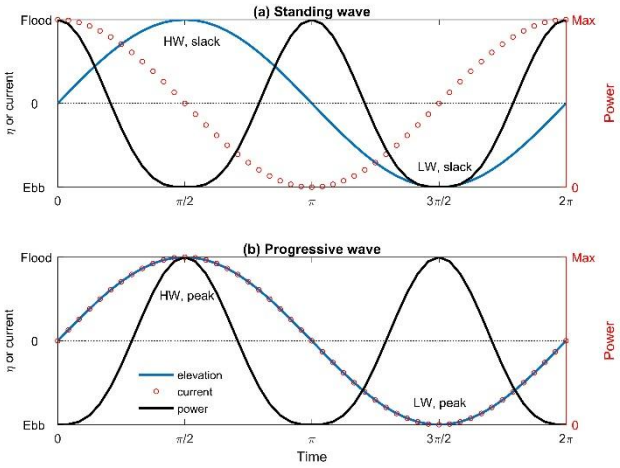

Figure 2: Phase relationship between tidal elevations (blue line) and tidal currents (red circles), for (a) standing and (b) progressive wave systems. Also shown is the power density (black lines), approximated using the absolute value of the velocity cubed, U^3, see Equation 3). Note the different scales on the left- and right axes.

3. Study region – the Irish Sea

The Irish Sea is a semi-enclosed mesoscale basin, characterised by strongly semi-diurnal Kelvin-type tides that are macro tidal in the east, with the tidal range exceeding 12 m at Avonmouth (Bristol Channel; Neill et al. 2009). In the west, one partial amphidromic system dominates, to the east coast of Ireland, which is a degenerate amphidrome (Pingree and Griffiths 1979). As a result, the Irish Sea contains both standing and progressive wave systems. Several regions have a significant tidal stream resource, and have been considered for commercial exploitation, including west and north of Anglesey, off the Pembrokeshire coastline, the Bristol Channel, and around Northern Ireland (Fig. 3). In these areas, the resource is often concentrated within narrow straits and around headlands and islands, where depth-averaged peak spring tidal currents are in excess of 2 m/s.

In recent years, there have been several existing and proposed tidal stream projects within the Irish Sea, including: Ramsey Sound, Llyn Peninsula, Anglesey-Skerries, Anglesey Demonstration Zone, Strangford Lough, Mull of Kintyre, Torr Head, and Fair Head (Fig. 3; Roche et al. 2016; Haverson et al. 2017), although some of these projects have stalled due to funding issues (e.g. Anglesey-Skerries). The Crown Estate has estimated that these areas have a potential combined installed capacity of 2-4 GW, although Lewis et al. (2015) suggested that the tidal stream resource could be even higher if deeper water and lower flow sites were developed, such as the partial amphidromic point off Ireland. While studies to predict performance have been carried out for many of these projects, optimal siting, resilient design, and the

interaction between the device, the resource, and the environment are topics of active research (Roche et al. 2016).

The Irish Sea is ideal for this study, as it experiences both standing and progressive wave systems within close proximity (Fig. 4) and, interestingly, both systems occur within regions of strong tidal currents that are potentially exploitable by tidal stream technologies (Uncles 1983; Pugh 1987). Within the Bristol Channel and much of the northern Irish Sea, including Liverpool Bay, the tide behaves as a standing wave (Lewis et al. 2014). Throughout much of the central and southwestern Irish Sea, a progressive wave is observed, where peak currents occur close to high or low water. This study characterises standing and progressive wave systems throughout the Irish Sea, and how these systems affect the tidal stream resource potential for both bottom-mounted and floating devices.

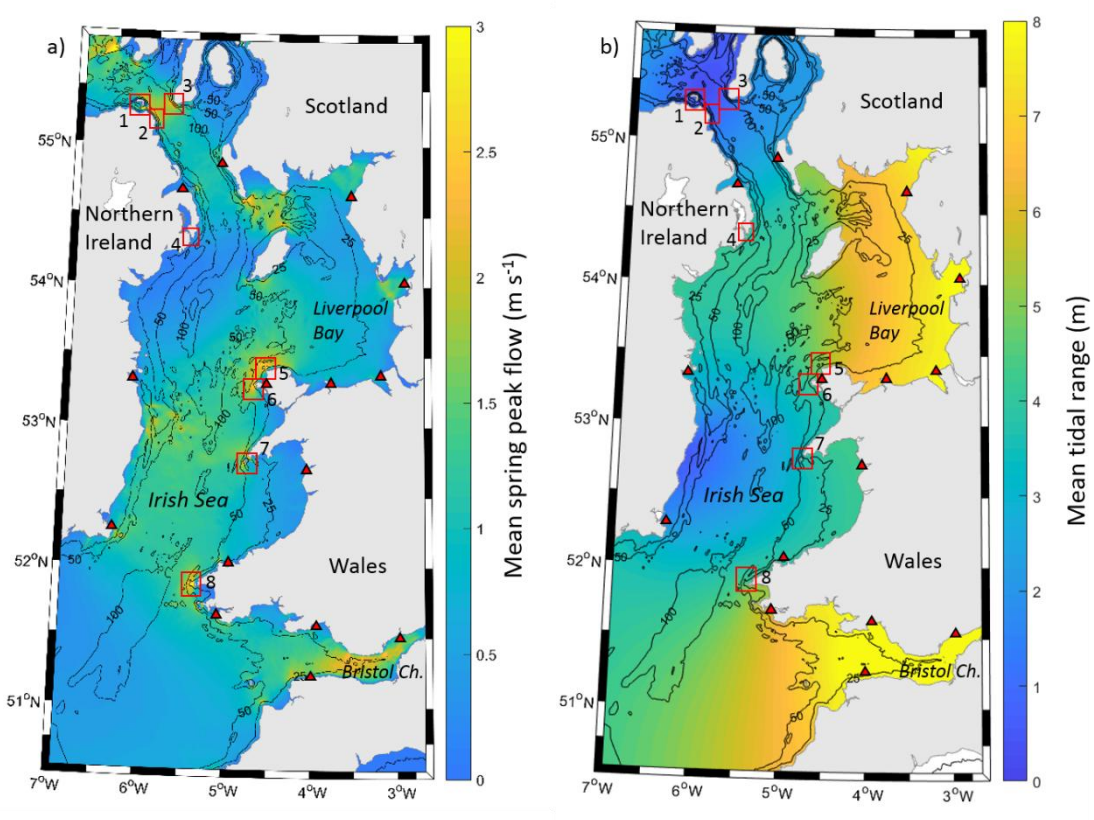

Figure 3: Domain extent of the Irish Sea model. Colour scale in (a) shows the mean spring peak depth-averaged velocities, and in (b) shows mean tidal range. Contour lines show bathymetry at mean sea level. Existing and proposed tidal stream projects are marked (red squares): (1) Fair Head; (2) Torr Head; (3) Mull of Kintyre; (4) Strangford Lough; (5) Anglesey-Skerries; (6) Anglesey Demonstration Zone; (7) Llyn Peninsula; (8) Ramsey Sound. Tide gauge (National Tidal and Sea Level Facility 2012) locations used for validation are also marked (red triangles).

4. Three-dimensional ROMS model

We apply the Regional Ocean Modeling System (ROMS) to the Irish Sea. A number of recent studies have used ROMS to successfully evaluate the marine renewable energy resource around the United Kingdom and northwest European shelf seas (e.g. Neill et al. 2014a; 2014b; Hashemi et al. 2015b). ROMS is an open-source, 3D, free-surface, terrain-following, primitive equations model, suitable for investigating a broad range of oceanographic processes on various temporal and spatial scales, including regional and coastal domains. The finite-difference approximations of the Reynolds-averaged Navier-Stokes equations are implemented using the hydrostatic and Boussinesq assumptions. The numerical algorithms of ROMS are described further in Shchepetkin and McWilliams (2005).

4.1. Model application to the Irish Sea

The domain extent for the Irish Sea tidal model was 7.0°W to 2.6°W and 50.5°N to 55.8°N at a resolution of approximately 1/120° longitude and with variable latitudinal resolution (~1/190°–1/210°, i.e., ~550 m grid spacing), using a horizontal curvilinear grid. The tidal model was set to have ten layers in the vertical sigma coordinate, using the coordinate system of Shchepetkin and McWilliams (2005). The depths of the layers were approximately 1, 3, 8, 15, 25, 45, 60, 75 and 90% of the water depth at each grid point. For example, for water depths of 30 m (tidal stream devices are typically designed for depths of 20-50 m), the minimum (maximum) thickness of a vertical layer was 0.3 m (6 m).

The bathymetric grid for the Irish Sea was derived from gridded Admiralty bathymetry data (digimap.edina.ac.uk), available at 200 m resolution, and it was corrected from Chart Datum to MSL. A minimum water depth of 8 m was set in the model, and so intertidal zones were not simulated. The exclusion of intertidal processes is not expected to have a significant influence on the tidal energy sites further offshore (water depths > 20 m). The model was forced at the boundaries using surface elevation (Chapman boundary conditions) and the *u* and *v* components of depth-averaged tidal current velocities (Flather boundary conditions), derived from FES-2014 (Finite Element Solution) which is a product derived from satellite altimetry data (Aviso 2012), available globally at a resolution of 1/16°. Tidal forcing consisted of the primary tidal constituents, namely M_2, S_2, N_2, K_1, O_1 and P_1.

The option for quadratic bottom drag scheme was implemented using a bottom drag coefficient (C_D) of 0.003, which is consistent with previous studies where ROMS was used to simulate tidal flows in tidally energetic areas (e.g. Robins et al. 2015, Ward et al. 2015). The coefficients of vertical harmonic viscosity and diffusion were computed

using the generic length scale (GLS) turbulence closure scheme model tuned to K-epsilon (p=3, m=1.5, and n=-1) (Umlauf and Burchard 2003; Warner et al. 2005; Thyng et al. 2013). Allowing for a 2-day model spin-up, 30 days of model simulations were analysed.

4.2. Model validation

Simulated surface elevations for the Irish Sea model were compared with observations at 15 coastal tide gauge locations distributed throughout the model domain (National Tidal and Sea Level Facility 2012). Simulated principal lunar (M_2) and solar (S_2) semi-diurnal tidal constituents were calculated at the grid point nearest to each tide gauge location using harmonic analysis (T_TIDE; Pawlowicz et al. 2002), and compared with corresponding tidal constituents derived from the observed data. The root mean square error (RMSE) for the 15 tide gauges was 0.1 m (Scatter Index, SI = 5%) in amplitude and 4° (SI = 2%) in phase for $\mathbf{M_2}$, and 0.04 m (SI = 5%) in amplitude and 3° (SI = 1%) in phase for $\mathbf{S_2}$, where the scatter index is the RMSE normalised by the mean of the data.

To validate the tidal current speeds simulated by the Irish Sea model, published current data from 21 offshore current meters were used (Jones 1983; Davies and Jones 1990; Young et al. 2000). Tidal harmonic analysis (T_TIDE, Pawlowicz et al. 2002) was used to compare tidal constituents (M_2 and S_2) between the data and the simulated depth-averaged current speed at the grid point nearest to each current meter location. The RMSEs of the $\mathbf{M_2}$ tidal currents were 3.8 cm/s in amplitude and 6° in phase, and were 1.3 cm/s and 6° in phase for the $\mathbf{S_2}$ tidal currents. The model was found to validate well when compared with the performance of other models of the region, which were of a similar spatial scale (e.g. Neill et al. 2010; Lewis et al. 2017). No particular regions of the model validated better with respect to tidal elevation/current meter data, i.e. there was no geographical bias.

5. Results

5.1. Standing and progressive wave systems

Firstly, we calculated the nature of the tidal waves in the Irish Sea, categorised as either standing or progressive wave systems. We calculated the time difference (in hours) between the second simulated high water (T_{HW}) and the closest preceding or succeeding simulated peak current flow (T_{PV}), based on the M_2 constituent only (which has a period of 12.42 hours), i.e. representative of mean tides:

$$\Delta T = abs(T_{HW}-T_{PV}) \quad (1)$$

We define standing wave systems to be where slack water occurs near high and low water, i.e., ΔT is maximal (2-3 hours). For M_2 only, as considered here, each hour time difference equates to the tidal elevations and velocities being out of phase by approximately 30°, e.g. where ΔT = 3 hours, M_2 elevations and velocities are the maximal 90° out of phase. In contrast, we define progressive wave systems to be where peak flows occur near high and low water, or where ΔT is minimal (e.g. < 1 hour, M_2 elevations and velocities are < 30° out of phase). Here we define the partially-progressive regions as having 1 < ΔT < 2 hours. See definitions in Table 2.

The spatial distribution of standing and progressive wave systems is shown in Fig. 4. South Wales and the Bristol Channel, and the majority of the northern Irish Sea, are characterised as standing wave systems, whilst tides in the central Irish Sea are mainly progressive. The several proposed tidal stream sites within this region are situated in varying progressive/standing tidal wave environments (Fig. 3). We analyse the results in Fig. 5, which shows the total coverage of the Irish Sea (areal extent in the model domain of ~5×10^6 km^2) defined in terms of standing and progressive wave systems and the corresponding peak M_2 current speeds. The peak M_2 current speeds are of more relevance to tidal stream resource characterisation than peak (spring) current speeds, since they can be scaled up to give an approximate representation of the long-term (e.g. annual) resource. Of the model domain considered, 14% of the areal extent had peak (depth-averaged) M_2 flows greater than 1 m/s, over half of which was characterised by standing wave systems (see Table 2). Of these areas (M_2 currents > 1 m/s) standing wave systems tended to be in shallower waters (mean water depth of 45 m) than progressive (mean water depth of 68 m). Although significantly less of the Irish Sea was characterised as a progressive wave tidal system compared with a standing wave system, there is little difference in the areal extents of standing/progressive wave systems with (depth-averaged) M_2 flows greater than 2 m/s (Table 2).

Table 2. Definition of tidal wave systems, based on time difference between high water and closest preceding or succeeding peak current flow, and areal extent of the Irish Sea model domain of each.

Regime	Phase difference (ΔT, hours)	Areal extent of Irish Sea (%)	Peak M_2 flows >1 m/s (as % of Irish Sea)	Peak M_2 flows >2 m/s (as % of Irish Sea)
Progressive	≤ 1	16	2.4	0.5
Partially-progressive	1 < ΔT ≤ 2	32	3	0.35
Standing	> 2	52	8	0.6

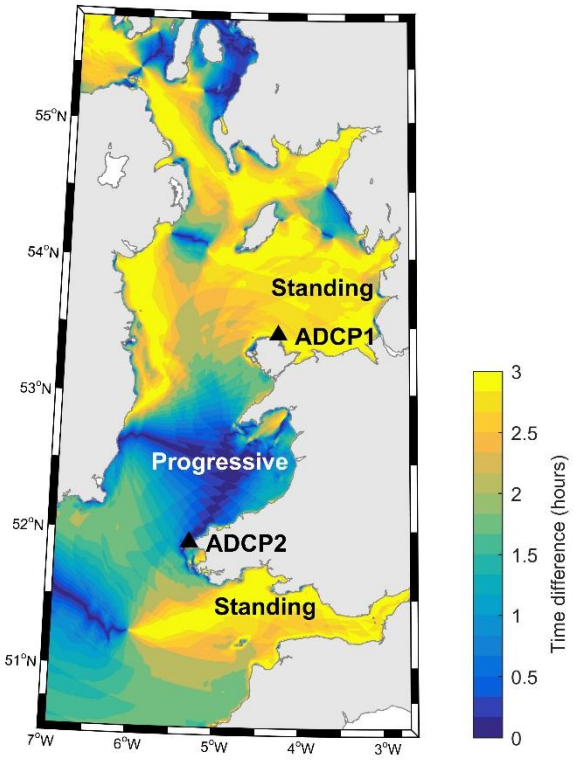

Figure 4: Time difference (ΔT in hours) between high water and peak M_2 current speeds in the Irish Sea. ΔT is given as coloured contours in 10-minute intervals. Black triangles show the locations of ADCP1 and ADCP2.

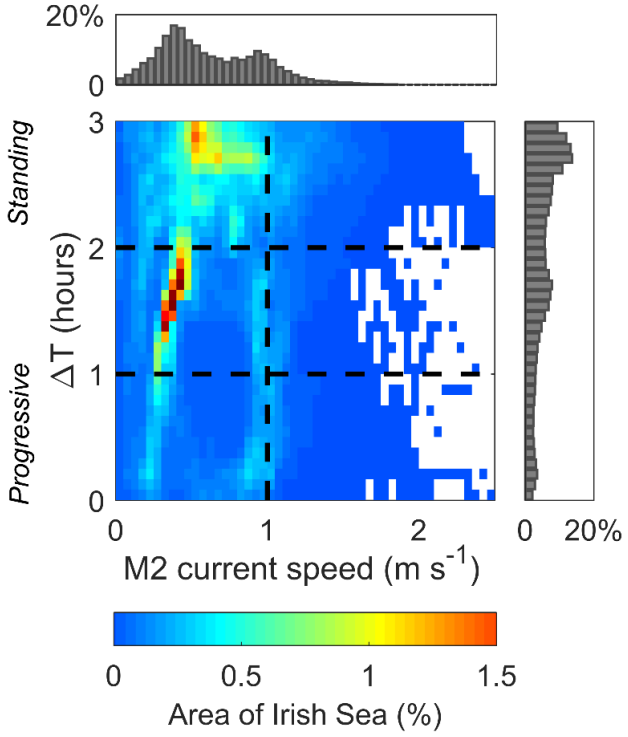

Figure 5: Colour matrix showing areal extent of the Irish Sea (%), distributed in terms of peak depth-averaged M_2 current speeds and standing/progressive wave systems. The top panel shows the distribution in terms of peak M_2 current speeds only (i.e. summing the matrix columns). The right panel shows the distribution in terms of the nature of the wave system only (i.e. summing the matrix rows). As an example interpretation, the majority of the Irish Sea experiences standing wave systems ($\Delta T >$ 2 hrs) with peak M_2 current speeds less than 1 m/s. The vertical dashed black line highlights M_2 current speeds > 1 m/s (regarded as a minimum threshold for tidal stream sites) and the horizontal dashed black lines differentiate between standing, partially-progressive and progressive wave systems.

5.2. Resource variability in the water column

To visualise some of the variability in tidal energy that can be extracted by floating and bottom-mounted devices, two example sites have been investigated in the southern Irish Sea (Fig. 6). Site 1 (in the Bristol Channel) has a mean water depth of 31 m, mean flows of ~0.8 m/s and represents a standing wave system where ΔT = 2.6 hrs. Site 1 is also characterised by a large tidal range, in excess of 8 m at springs. Site 2 (off St. David's Head, SW Wales) has a mean water depth of 28 m, mean flows of ~1.3 m/s and represents a progressive wave system where ΔT = 0 hrs. Tidal current ellipses at both sites are rectilinear, i.e. the direction of the ebb current is ~180^o from the flood current direction, and so suited to the installation of horizontal axis turbines.

From the model simulations, we extracted tidal elevation and velocity time series (over 30 days) from Site 1 and Site 2, plotted in Figs. 6a and 6b, respectively (note that Fig. 6 only shows a 12 hour period during spring tides). At Site 1 (standing wave), peak current speeds are broadly comparable during the flood and ebb phases of the tide (depth-averaged magnitudes of ~1.8 m/s). This tidal symmetry would ensure similar tidal energy extraction potential during both phases of the tidal cycle. At Site 2 (progressive wave), the peak current speeds at high water are stronger (up to 3 m/s) than at low water (up to 2.5 m/s), due to enhanced frictional influences at low water (since tidal range is around 4 m at springs, ~15% of mean water depth). Site 2 is also shallower than Site 1, which could contribute to the asymmetry. Such asymmetry in tidal currents over a tidal cycle would lead to asymmetries in power generation from this site, and highlights the need for resource assessments to consider the phase relationship between tidal currents and elevations at a more fundamental level. It is expected that most progressive wave sites are associated with higher degrees of current asymmetry over a tidal cycle than at standing wave sites. To test this we compared ΔT (i.e., standing or progressive) with M_4-generated tidal asymmetry, resulting from the phase relationship between the M_2 and M_4 tidal constituents (Pingree and Griffiths 1979). The degree of asymmetry, represented as an index from

0 to 1, was calculated using the model output for the entire Irish Sea. Using tidal harmomic analysis to extract the M_2 and M_4 tidal phases (Ø), we calculated the phase relationship $2\emptyset(M_2) - \emptyset(M_4)$; see Robins et al. (2015) for further details. The association between tidal asymmetry and progressive tidal waves sites was found to generally be true, although with a large degree of variation (Fig. 7).

The tidal kinetic energy power density (PD, in W/m^2) is a means of characterising the potential tidal stream resource of a location and can be calculated as follows:

$$PD = \tfrac{1}{2} \rho U^3 \quad (3)$$

where ρ=1025 kg/m^3 is the water density and U is the instantaneous velocity in m/s. Firstly, for the standing wave system at Site 1, the power density was calculated for a bottom-mounted ('fixed') device at a fixed mid-depth position relative to MSL (i.e. ~16 m above bed, indicated by the horizontal dashed black line in Fig. 6a). Next, the procedure was repeated for a floating device ('depth-varying') at a water column position that varies with the surface elevation (i.e., solid black curve in Fig. 6a). (Note: the time-averaged hub-height positions of both devices were equal.) The resulting power density values for both scenarios are shown in Fig. 6c. Finally, the whole procedure was repeated for the progressive wave system at Site 2 (fixed depth ~13 m above bed, Figs. 6b and 6d). Percentage differences discussed below refer to net power density over the 30-day simulation.

At times when the floating device was higher in the water column than the bottom-mounted device it experienced stronger flows and, hence, the potential to generate more instantaneous power than the bottom-mounted device (assuming equal hypothetical device efficiency). At Site 1 (standing wave), the net difference in power density between the two scenarios was small over the tidal cycle, although the bottom-mounted scenario encountered < 0.5% more available power density. A more complex pattern was evident at Site 2. The progressive nature of the tidal signal led to asymmetrical power density: greater during peak flood flow at high water, and markedly less during peak ebb flow at low water (Fig. 6d). This implies that progressive wave systems would generate unequal power between the flood and ebb phases of the tidal cycle (regardless of hub height). For Site 2, although the net difference in power density between the two scenarios was small over the tidal cycle, the floating scenario encountered 0.5-1% greater power density than the bottom-mounted scenario. As expected, the asymmetry, which would translate into asymmetrical power generation, was more pronounced for the floating scenario (Fig. 6d).

For the results to remain non turbine-specific, we only considered a point depth in the timeseries, and not the potential swept area of a turbine. For example, for a turbine with diameter 10 m, the tidal currents may vary considerably over that 10 m

of the water column. At Site 1 (standing), we found that the power density calculated at 5 m above the mid-depth was 36% more than at 5 m below the mid-depth, for both bottom-mounted and floating scenarios. At Site 2 (progressive), the power densities at 5 m above the mid-depth were 37% (bottom-mounted) and 40% (floating) more than at 5 m below the middepth. Interestingly, the most significant difference between floating and bottom-mounted at these depths was at 5 m below the middepth at Site 2, where the floating tidal device encountered 1.8% greater power density than the bottom-mounted scenario over the 30 day simulation. In contrast, at 5 m above the middepth at Site 2, the bottom-mounted device encountered a minimal 0.2% higher power density. This suggests that if future studies were to consider the swept area of a turbine, rather than a point depth, then the discrepancy between the bottom-mounted and floating devices could be even greater in the progressive wave regions.

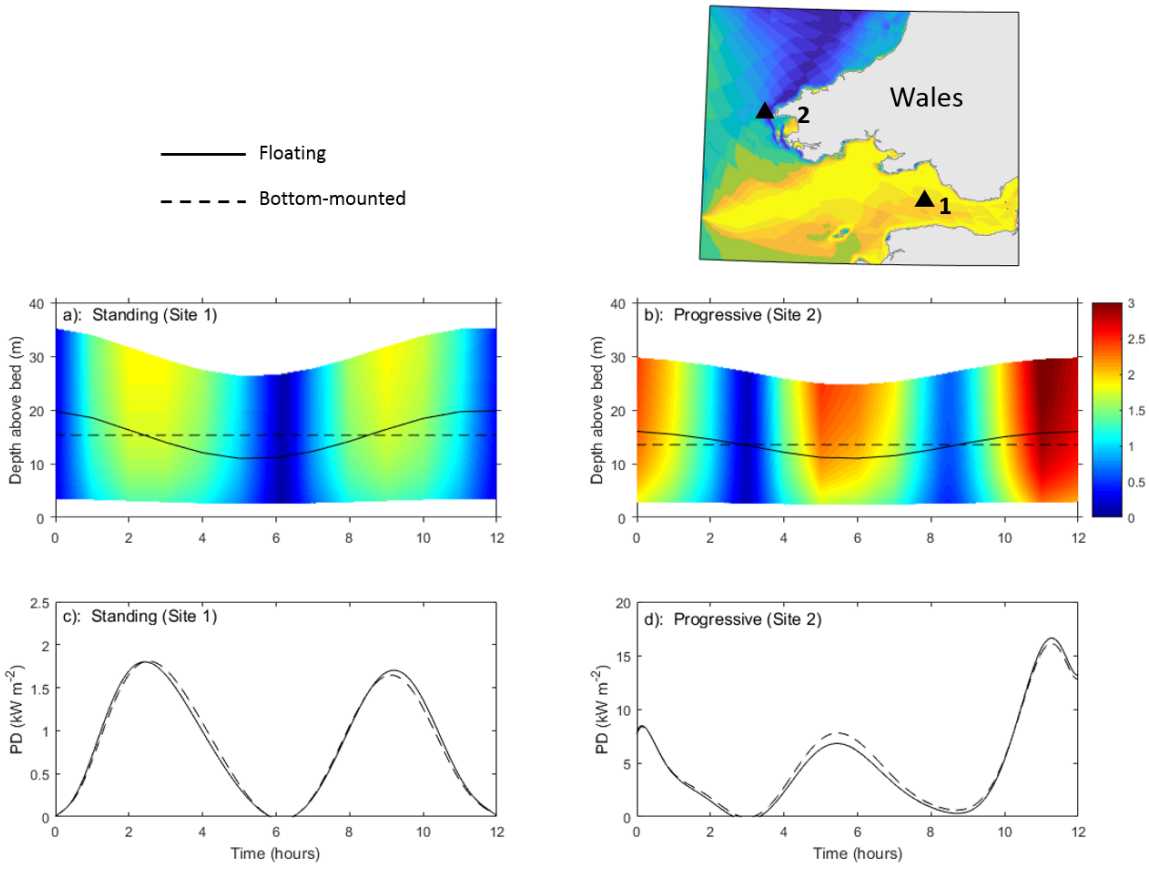

Figure 6: Time series of simulated tidal current speeds and elevations at (a) Site 1 (standing wave) and (b) Site 2 (progressive wave). The location of these time series is plotted in the top right panel (see Fig. 4 for reference). Panels (a) and (b) also show the mid-depth position of a potential bottom-mounted device (dashed black line) and floating device (solid black curve). The power density along these lines is plotted in (c) and (d), respectively.

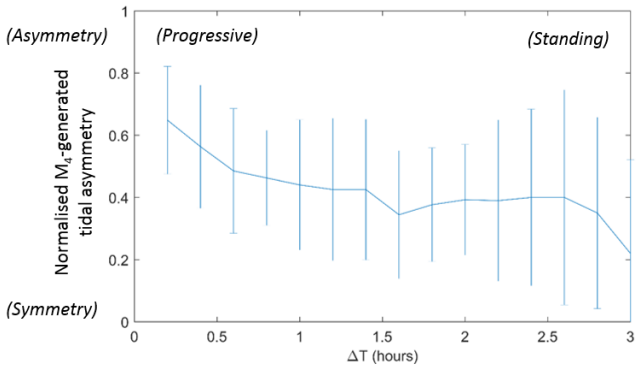

Figure 7: Relationship between standing and progressive wave systems (ΔT, averaged for 12 minute bins) and M_4-generated tidal asymmetry, for locations in the Irish Sea where peak M_2 velocities exceeded 1 m/s. Tidal asymmetry was calculated based on the relationship $2\emptyset(M_2) - \emptyset(M_4)$, where $\emptyset$ is the tidal phase. The Y-axis has been normalised so that zero signifies tidal symmetry and one signifies maximal tidal asymmetry; see Robins et al. (2015) for further details. Error bars denote one standard deviation from the mean.

5.3 Power density calculated from *in-situ* tidal current data

Here we use data from two ADCPs (acoustic Doppler current profilers), collected off the north coast of Anglesey (ADCP1, ΔT ~ 3 hours) and north of Pembrokeshire (ADCP2, ΔT ~1 hour) (locations shown in Fig 4). ADCP1 (standing wave site) was an upward-looking 4-beam Teledyne RDI Workhorse Sentinel 600 kHz ADCP, deployed during February-March 2014 (MSL ~38 m). Velocities were recorded at 0.4 Hz, in 2 minute ensembles, at 1 m bins throughout the water column. ADCP2 (progressive wave site) was the same instrument as ADCP1, deployed during October 2014 (MSL ~40 m). Velocities were recorded at 0.5 Hz, in 10 second ensembles, at 1 m bins throughout the water column. Using current data from these two ADCPs, we further consider the differences in power density encountered by bottom-mounted and floating devices (Fig. 8). We repeated the power density calculations (Section 5.2) for floating and bottom-mounted devices. The most significant results here are: i) at ADCP2 (progressive), there was a greater variation with depth in the difference in power density for floating versus bottom-mounted than at ADCP1 (standing); ii) at ADCP2, there was greater velocity-asymmetry (and hence power-asymmetry) over a tidal cycle, which was exacerbated for floating; and finally iii) at ADCP2, the bottom-mounted device was more strongly favourable over the floating device than at ADCP1. Interestingly, at both sites considered, the bottom-mounted hub remained favourable even in the top half of the water column, with the exception of at 30 m hub height (above the bed at ADCP1), which is less than 10 m below the MSL.

We include an example comparison of power density between the two ADCP sites (and hence flow regimes) and of the power density encountered by theoretical floating versus bottom-mounted devices at those sites. To note is that these data are site-specific and the key results of the comparison are detailed above. At the mid-depth of both ADCP sites (i.e., mid-depths of 19 m for ADCP1, 20 m for ADCP2), the bottom-mounted device encountered more power density than the floating device which tracked the surface elevation (0.3% more for ADCP1, 0.7% more for ADCP2, i.e., a greater difference at the progressive site). At both ADCP sites the theoretically bottom-mounted hub was favourable throughout the water column (Fig. 8b and 8d), with greater power density (up to 3% more) than the floating device in the bottom half of the water column at ADCP2.

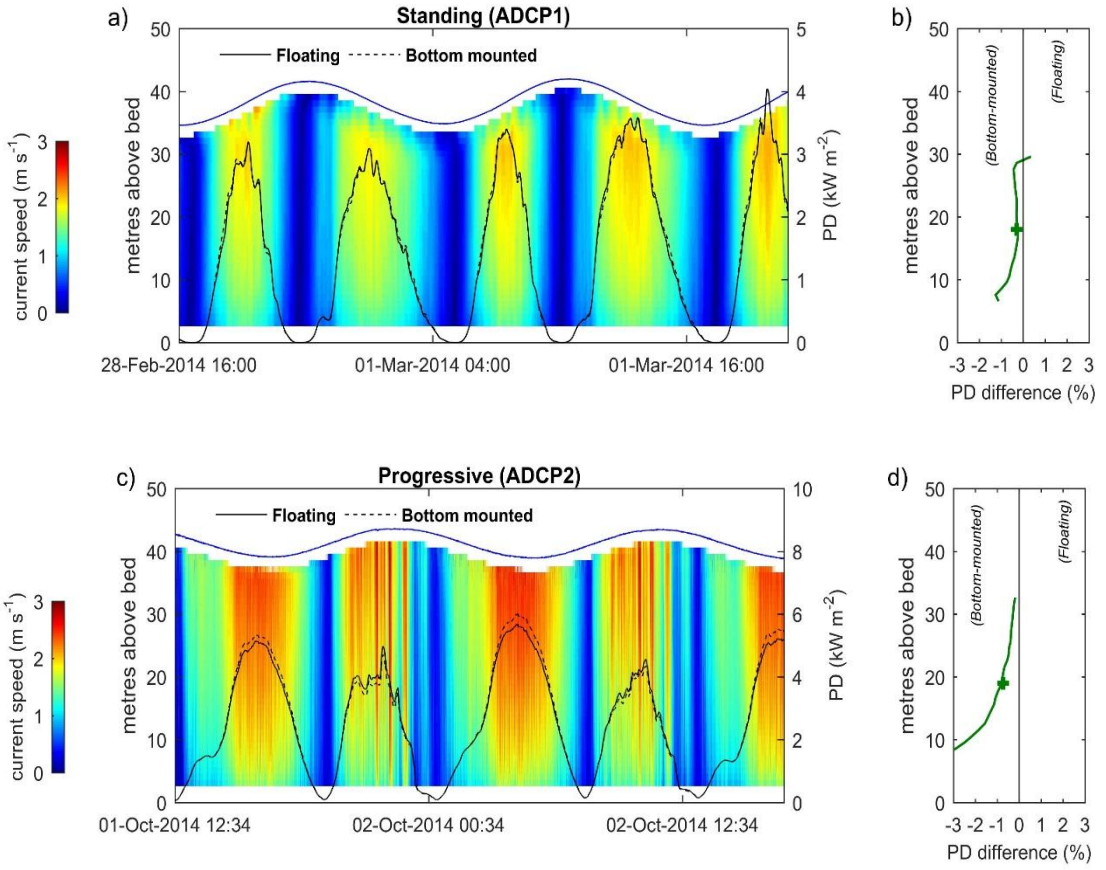

Figure 8. Time series of observed tidal current speeds and elevations during spring tides at (a) ADCP1 (standing wave) and (c) ADCP2 (progressive wave). The black lines on the timeseries indicate the power density (right axis) calculated at the mid-depth for floating (solid) and bottom-mounted (dashed) devices. The right two panels indicate the percent difference in power density (PD) at (b) ADCP1 and (d) ADCP2, varying with water depth, where negative/positive difference in PD indicates bottom-mounted/floating devices favoured, respectively.

5.4 Power density: Irish Sea

The analysis was then extended to the entire Irish Sea. Using the simulated 3D velocities, the percentage differences in net power density (over 30 days) between the floating (depth-varying) and bottom-mounted (fixed) scenarios were calculated, for three different hub heights: 10 m, 15 m, and 20 m below sea surface (Fig. 9). For each scenario, the floating hub height varied relative to the sea surface elevation and the bottom-mounted hub height position was fixed relative to MSL.

Where there is a positive difference in power density (red areas in Fig. 9), bottom-mounted devices were favourable over floating devices, i.e. higher power density for

bottom-mounted devices at a fixed depth. Conversely, areas with a negative difference in power density (blue areas in Fig. 9) denote where floating devices are favourable. General results show that net differences in power density (over a 30 day period) were mostly small (<0.25%) between the two scenarios – and the pattern simulated at a 10 m hub height was remarkably similar to that at 15 m and 20 m other than a change in sea space due to the depth constraint (Fig. 9). Of most interest to developers are sites with strong tidal currents: notable regions with peak depth-averaged M_2 flows greater than 1 m/s and large differences in power density included the following (marked on Fig. 9): (1) ±2% off the Stranraer Peninsula, Scotland; (2) ±2.5% around the Isle of Man and in north-eastern Liverpool Bay; (3) +2% off St. John's Point, Northern Ireland; (4) ±2.5% through Bardsey Sound, Wales; and (5) ±2.5% off South Wales (Fig. 9). These key sites are transitional regions from standing to progressive waves (Fig. 4), where strong tidal flows were either deflected around headlands and islands or constrained within channels. These sites are also in relatively shallow water (generally < 50 m, see Fig. 1).

In fact, many shallow water sites tended to experience greater differences in power density compared with deeper sites (Fig. 10a) – because shallow sites experience greater differences in stream flow over the vertical. Furthermore, sites with large tidal ranges (Fig. 3b) also tended to experience greater differences in power density between the floating and bottom-mounted scenarios (Fig. 10b), again due to the larger differences in stream flow over the vertical. These important results demonstrate the sensitivity of large tidal range sites in shallow water to the type of tidal stream turbine used, and are applicable to any potential tidal stream energy site, globally. Further still, although the differences in power density presented here are small, the implication is for potentially considerable differences is power generation over the lifetime of a tidal stream device.

For Irish Sea locations where simulated mean flows exceeded 1 m/s, percentage differences in power density ranged from -1% to +2.5%, and most locations (~60%) had a positive percentage difference, hence favouring bottom-mounted devices. Strongly progressive regions (ΔT <0.5 hours) again tended to encounter positive percentage differences in power density (Fig. 11). This implies that, during peak flow at high water when the floating hub height is above the bottom-mounted hub height, the stronger flows and increased power density encountered by the floating device did not compensate for the reduced flows and power density encountered during peak flow at low water – hence, overall, the bottom-mounted hub height encountered higher mean tidal currents than the floating devices in progressive wave systems. However, for other types of tidal wave – partially-progressive through to standing – no significant correlation between phase relationship and the difference in power density was detected. This result was expected for standing wave systems,

where flood and ebb peaks in flow are often similar; hence favouring neither floating nor bottom-mounted hub heights. For partially-progressive regions, the overall net power density is likely influenced by a combination of processes, for example, tidal asymmetry. Nevertheless, our comparison did always produce a difference in power density between floating and bottom-mounted hub heights, which we argue should be considered in more detailed resource assessments.

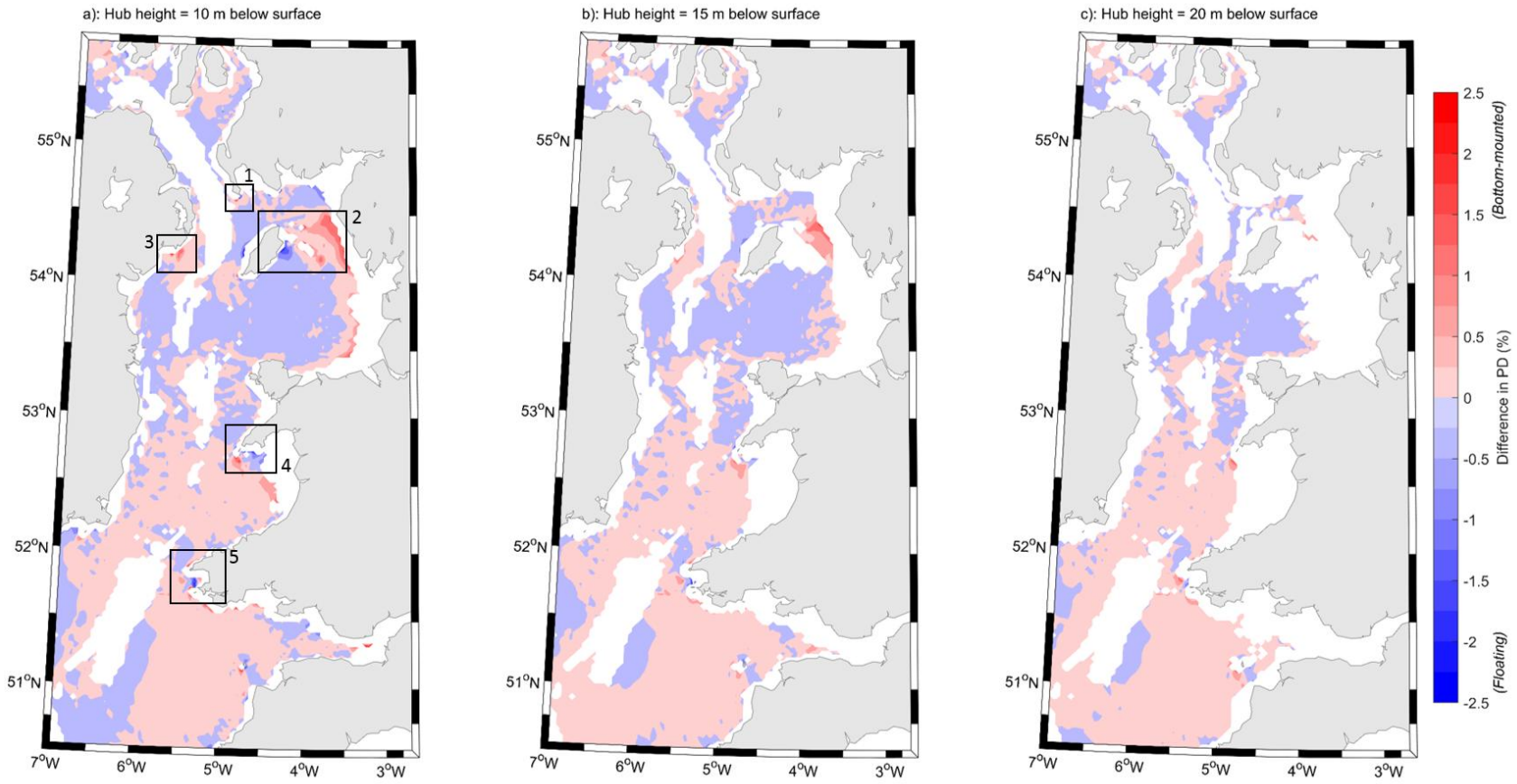

Figure 9: Difference (in %) of power density (in kW/m^2) between floating and bottom-mounted tidal stream devices, calculated using simulated tidal current speeds over a 30 day period throughout the Irish Sea. Panel (a) compares flows encountered by a floating device (10 m below the changing sea surface) with flows encountered by a bottom-mounted device (10 m below the fixed mean sea level). Panels (b) and (c) show similar comparisons at 15 m and 20 m depths below surface. Deep water (>100 m) and shallow water ((a) <20 m, (b) <30m, (c) <40m) were not analysed (white regions).

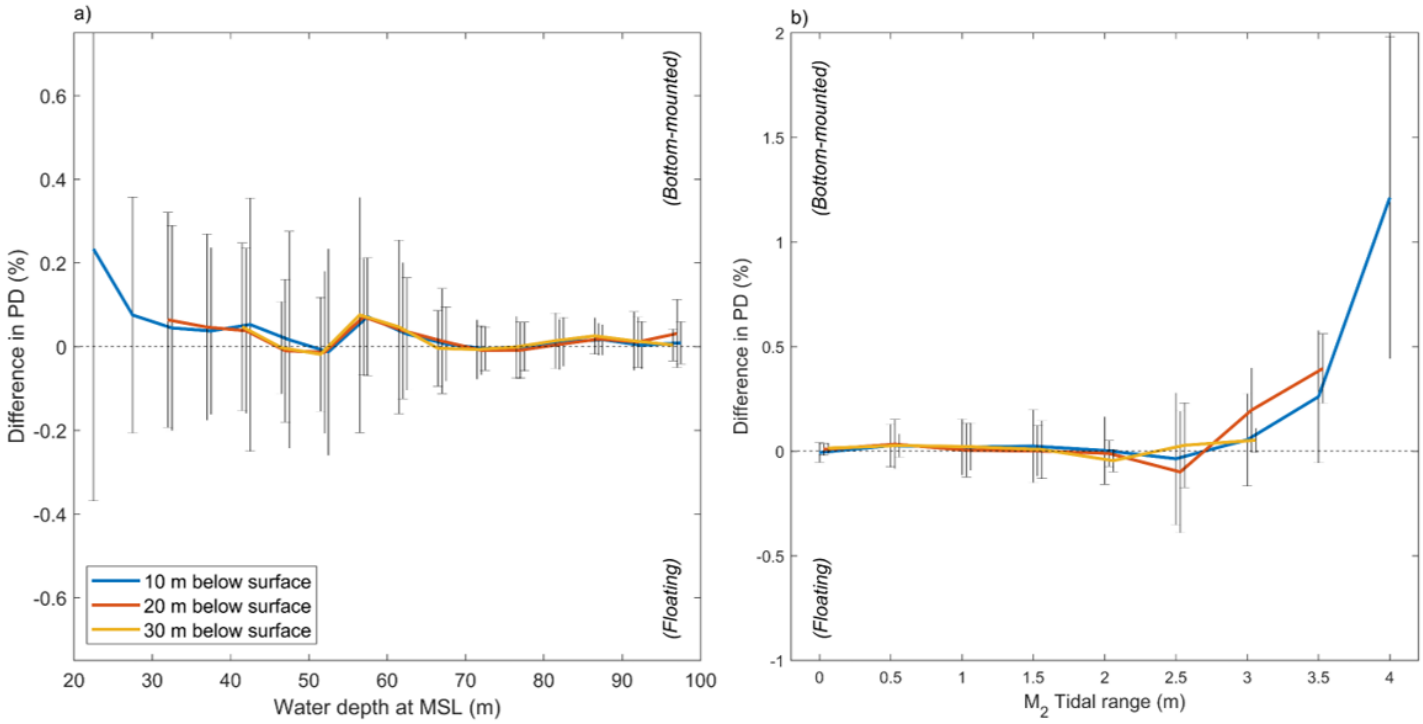

Figure 10: Relationships between (a) water depth and percentage difference in power density (PD), and (b) tidal range and percentage difference in power density, for three different depths below the surface. The analysis corresponds to regions of the Irish Sea model where simulated depth-averaged M_2 flow exceeds 1 m/s. Error bars denote standard deviation from the mean. Positive percentage differences in power density indicate greater energy available for extraction by bottom-mounted devices than by floating devices at that depth below surface, and vice versa.

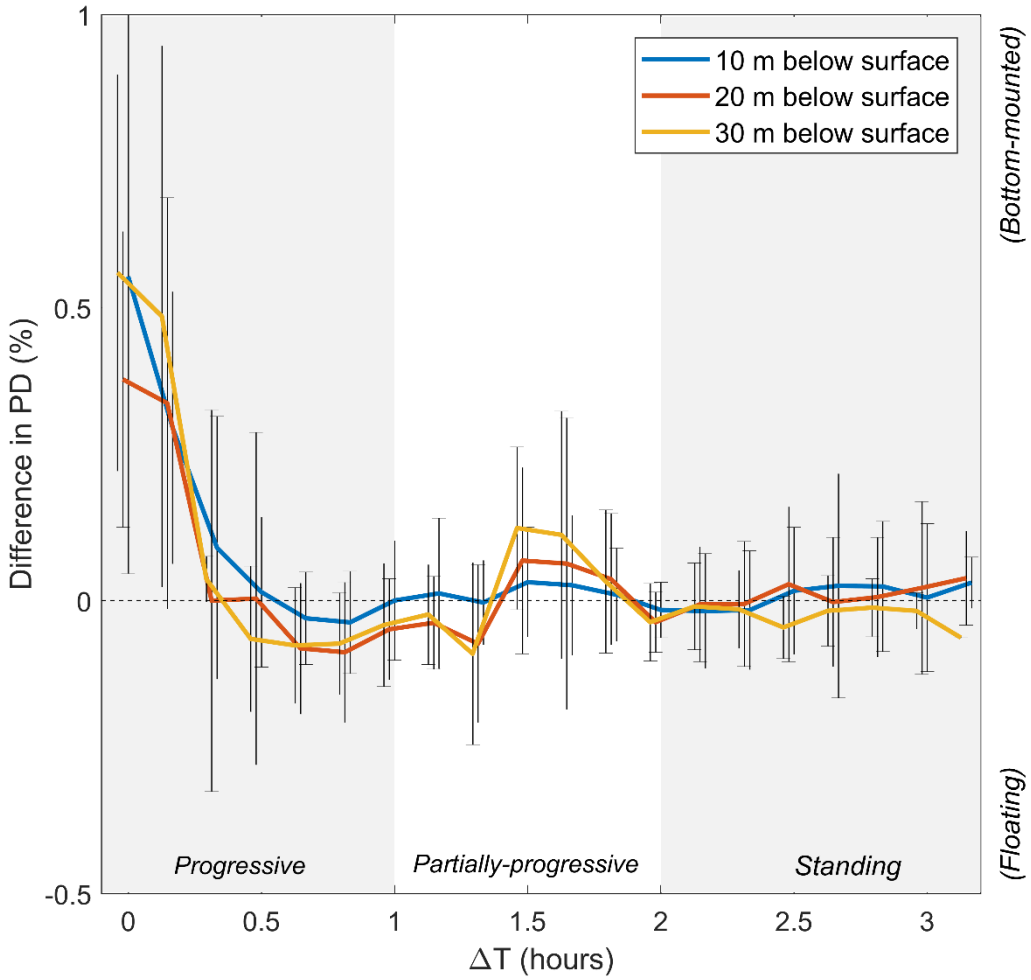

Figure 11: Relationship between the nature of the tidal wave (ΔT) and percentage difference in power density, for three different depths below surface. The analysis corresponds to regions of the Irish Sea model where simulated depth-averaged M_2 flow exceeds 1 m/s. Error bars denote one standard deviation from the mean. Positive percentage differences in power density indicate greater energy available for extraction by bottom-mounted devices than by floating devices at that depth below surface, and vice versa.

6. Discussion

Beneath the wind and wave influenced surface layer of the ocean, velocities are strongest higher up in the water column and decrease with depth broadly in accordance with the $1/7^{th}$ power law velocity profile (Lewis et al. 2014; 2017). Based on this knowledge, the optimal (practical) hub height for a bottom-mounted tidal stream device can be determined, and the long-term resource estimated. Our study has shown that progressive wave systems in shallow water will encounter stronger peak flows at high tide than at low tide due to differing frictional influences, and hence tidal energy devices that intercept the flow in these regions would lead to

asymmetrical power generation over the tidal cycle, with more power generated at high water than at low water. For floating (surface tracking) devices in shallow progressive systems, the asymmetry in the power density was enhanced further. This generally resulted in reduced overall power density compared with a bottom-mounted device at a similar hub height; i.e. a greater reduction in current flow speeds (which would translate into decreased power) at low water than increased flow speeds (and hence power) at high water. In effect, the power density asymmetry is not caused by the progressive nature of the tidal system, but by the tidal asymmetry it is generally accompanied by. If we also consider that turbine rated speeds could be exceeded for some of the tidal cycle (e.g. during peak flow at high tide), then the difference in *technical* power generation (over a tide) between bottom-mounted and floating devices could feasibly be even greater than predicted here (Sanchez et al. 2013). There is also no consideration here of rated speeds of individual turbines, which could contribute further to differences in power generation from bottom-mounted or floating devices. For example, it is possible that lower tidal current speeds at low water, which have been shown here to be exacerbated for floating devices in progressive wave systems, may not be high enough to exceed the rated speed of a device, potentially further augmenting the difference in power generation from the different devices.

For standing wave systems, peak flood and ebb velocities tend to be comparable in magnitude because they occur in similar total water depths. Therefore, in general, over a tidal cycle both bottom-mounted and floating devices lead to comparable power densities when positioned at similar hub heights. We also note that most regions of large tidal range in the Irish Sea are typically standing wave systems (Fig. 5), leading to a rather counter-intuitive result that net power generation in these regions is not sensitive to the turbine mooring scheme (floating or bottom-mounted), even though the different schemes will encounter different instantaneous stream flows due to the large tidal range. Indeed, power generation on sub-tidal timescales will be sensitive to the mooring scheme.

One obvious advantage of floating devices is that in relatively deep waters, e.g. > 50 m, they can be positioned higher up in the water column than bottom-mounted devices, due to practical limitations of installing expensive support structures. Floating devices would encounter stronger flows and generate more power in this case (Sanchez et al. 2014a). This would be the case for both standing and progressive wave systems, although it should be noted that deeper waters tend not to have sufficiently strong tidal flows for the majority of devices currently being developed.

Analysis of all resource characterisation studies should account for the uncertainties in both the forcing data (e.g. bathymetry, tidal forcing, and atmospheric forcing) and

in model parameterisations (e.g. velocity profile parameterisation: Lewis et al. 2017; and bed roughness parameterisation: Davies and Robins 2017). For coupled model applications and future predictions, these uncertainties are exacerbated (e.g. Xie et al. 2015). In the present study it has been assumed that the current speed at the hub height is representative of the current speeds in the area swept by the turbine rotor, and there has been no consideration of device efficiency. Turbine diameters vary significantly (e.g. Evopod floating device, 5 m diameter, Meygen bottom-mounted device 16 m diameter) and so calculation of power density over the swept area of a turbine has not been conducted, in order to ensure the results and overall findings remain generic and not turbine specific. We propose that in future work the vertical variability of current speed within the area swept by a turbine rotor should be accounted for in estimating the energy output. It would also be interesting for further studies to consider the sensitivity of the present results to the rotor diameter. Further, comparison of the potential environmental impacts between floating versus bottom-mounted devices, in either standing or progressive wave systems also needs to be addressed in future studies.

7. Conclusions

Tidal stream energy conversion is viable in regions with strong tidal currents, and such regions are often resonant standing wave tidal systems where peak flood/ebb currents occur in similar water depths during the rising/falling tides hence experiencing similar flow magnitudes. In such standing wave systems, turbines that are mounted to a floating platform would encounter a variable hub height that tracks the surface elevation and consequently would access the faster currents higher in the water column, although this appears to have a small net effect on theoretical power generation.

Some regions with strong tidal flows are progressive or partially-progressive in nature, meaning that peak currents occur close to high water and low water (rather than mid-way in between), and so can experience flow asymmetry over the tidal cycle due to increased frictional influences of the seabed at low water. This effect is exacerbated in shallow waters, and also where tidal ranges are large. In these regions, it will be important to recognise that floating devices that track the sea surface may encounter greater flow asymmetry over a tidal cycle (and hence generate greater power asymmetry) – but also generate less net power than bottom-mounted devices, largely because of the greater losses at low tide.

We suggest that floating platform schemes are generally well-suited to resonant standing wave tidal systems and also to deeper waters, but perhaps less well-suited to shallow progressive tidal systems than bottom-mounted devices. Our characterisation of the resource, at different water depths, is important for tidal stream developers for calculation of the potential resource variability as well as for design requirements of their technologies.

Acknowledgements

This work was undertaken as part of the SEACAMS and SEACAMS2 projects, which is part-funded by the European Union's Convergence European Regional Development Fund, administered by the Welsh Government. S. Neill and M. Lewis wish to acknowledge the support the Sêr Cymru National Research Network for Low Carbon, Energy and the Environment (NRN-LCEE). The model simulations were conducted on Supercomputing Wales (a collaboration between Welsh universities and the Welsh Government). Marco Piano, Ben Powell and Aled Owen provided invaluable support with the ADCP deployments.

References

Aviso. 2012. FES2012 was produced by Noveltis, Legos and CLS Space Oceanography Division and distributed by Aviso, with support from Cnes (www.aviso.altimetry.fr/).

Coles DS, Blunden LS, Bahaj AS. 2017. Assessment of the energy extraction potential at tidal sites around the Channel Islands. Energy 124: 171-186.

Commin AN, McClatchey J, Davidson MW, Gibb SW. 2017. Close-proximity tidal phasing for 'firm' electricity supply. Renewable Energy 102: 380-389.

Davies AM, Jones JE. 1990. Application of a three-dimensional turbulence energy model to the determination of tidal currents on the northwest European Shelf. Journal of Geophysical Research 95 (C10): 18143.

Davies AG, Robins PE. 2017. Residual flow, bedforms and sediment transport in a tidal channel modelled with variable bed roughness. Geomorphology 15: 855-872

Flather RA. 1976. A tidal model of the north-west European continental shelf. Memoires de la Society Royal des Sciences de Liege 6 series (10): 141-164.

Garrett C. 1972. Tidal resonance in the Bay of Fundy and Gulf of Maine. Nature 238: 441-443.

Guillou N, Neill, SP, Robins PE. 2018. Characterising the tidal stream power resource around France using a high-resolution harmonic database. Renewable Energy (in review).

Hashemi MR, Neill SP, Robins PE, Davies AG, Lewis MJ. 2015a. Effect of waves on the tidal energy resource at a planned tidal stream array. Renewable Energy 75: 626-639.

Hashemi, MR, Neill, SP, and Davies, AG. 2015b. A coupled tide-wave model for the NW European shelf seas. Geophysical & Astrophysical Fluid Dynamics, 109: 234-253.

Haverson D, Bacon J, Smith HC, Venugopal V, Xiao Q. 2017. Cumulative impact assessment of tidal stream energy extraction in the Irish Sea. Ocean Engineering 137: 417-428.

Iyer A, Couch S, Harrison G, Wallace A. 2013. Variability and phasing of tidal current energy around the United Kingdom. Renewable Energy 51: 343-357.

Jones J. 1983. Charts of O1, K1, N2, M2 and S2 Tides in the Celtic Sea including M2 and S2 Tidal Currents. Tech. rep.

Lewis MJ, Neill SP, Elliott AJ. 2014. Interannual variability of two offshore sand banks in a region of extreme tidal range. Journal of Coastal Research 31: 265-75.

Lewis MJ, Neill SP, Robins PE, Hashemi MR. 2015. Resource assessment for future generations of tidal-stream energy arrays. Energy 83: 403-415.

Lewis MJ, Neill SP, Robins PE, Hashemi MR, Ward SL. 2017. Characteristics of the velocity profile at tidal-stream energy sites. Renewable Energy 114: 258-272.

Li C, O'Donnell J. 2005. The effect of channel length on the residual circulation in tidally dominated channels. Journal of Physical Oceanography 35: 1826-1840.

National Tidal and Sea Level Facility. 2012. Real-time data - UK National Tide Gauge Network. (www.ntslf.org/data/uk-network-real-time).

Neill SP, Litt EJ, Couch SJ, Davies AG, 2009. The impact of tidal stream turbines on large-scale sediment dynamics. Renewable Energy 34: 2803-2812.

Neill SP, Scourse JD, Uehara K. 2010. Evolution of bed shear stress distribution over the northwest European shelf seas during the last 12,000 years. Ocean Dynamics 60: 1139-1156.

Neill SP, Hashemi MR, Lewis MJ. 2014a. Optimal phasing of the European tidal stream resource using the greedy algorithm with penalty function. Energy 73: 997-1006.

Neill SP, Hashemi MR, Lewis MJ. 2014b. The role of tidal asymmetry in characterizing the tidal energy resource of Orkney. Renewable Energy 68: 337-350.

O'Hara Murray R, Gallego A. 2017. A modelling study of the tidal stream resource of the Pentland Firth, Scotland. Renewable Energy 102: 326-340.

Pawlowicz R, Beardsley B, Lentz S. 2002. Classical tidal harmonic analysis including error estimates in MATLAB using T TIDE. Computers & Geosciences 28: 929-937.

Piano M, Neill SP, Lewis MJ, Robins PE, Hashemi MR, Davies AG, Ward SL, Roberts MJ. 2017. Tidal stream resource assessment uncertainty due to flow asymmetry and turbine yaw misalignment. Renewable Energy 114: 1363-1375.

Pingree RD, Griffiths DK, 1979. Sand transport paths around the British Isles resulting from M2 and M4 tidal interactions. Journal of the Marine Biology Association UK 59:497-513

Pugh DT. 1987. Tides, Surges and mean sea-level. Vol. 5. John Wiley & Sons, Ltd., Chichester.

Robins PE, Neill SP, Lewis MJ. 2014. Impact of tidal-stream arrays in relation to the natural variability of sedimentary processes. Renewable Energy 72: 311-321.

Robins PE, Neill SP, Lewis MJ, Ward SL. 2015. Characterising the spatial and temporal variability of the tidal-stream energy resource over the northwest European shelf seas. Applied Energy 147: 510-522.

Sanchez M, Carballo R, Ramos V, Iglesias G. 2014a. Energy production from tidal currents in an estuary: A comparative study of floating and bottom-fixed turbines. Energy 77: 802-811.

Sanchez M, Carballo R, Ramos V, Iglesias G. 2014b. Floating vs. bottom-fixed turbines for tidal stream energy: A comparative impact assessment. Energy 72: 691-701.

Sanchez M, Iglesias G, Carballo R, Fraguela JA. 2013. Power peaks vs. installed capacity in tidal stream Energy. IET Renewable Power Generation 7: 246-253.

Shchepetkin AF, McWilliams JC. 2005. The regional oceanic modeling system (ROMS): a split-explicit, free-surface, topography-following-coordinate oceanic model. Ocean Modelling 9: 347-404.

Thiébaut, M. and Sentchev, A., 2017. Asymmetry of tidal currents off the W. Brittany coast and assessment of tidal energy resource around the Ushant Island. Renewable Energy 105: 735-747.

Thyng KM, Riley JJ, Thomson J. 2013. Inference of turbulence parameters from a ROMS simulation using the k-ε closure scheme. Ocean Modelling 72: 104-118.

Umlauf L, Burchard H. 2003. A generic length-scale equation for geophysical turbulence models. Journal of Marine Research 61: 235-265.

Uncles RJ. 1983. Modeling Tidal Stress, Circulation, and Mixing in the Bristol Channel as a Prerequisite for Ecosystem Studies. Canadian Journal of Fisheries and Aquatic Sciences 40 (S1): s8-s19.

Waldman S, Baston S, Nemalidinne R, Chatzirodou A, Venugopal V, Side J. 2017. Implementation of tidal turbines in MIKE 3 and Delft3D models of Pentland Firth & Orkney Waters. Ocean & Coastal Management. 2017 May 7.

Warner JC, Sherwood CR, Arango HG, Signell RP. 2005. Performance of four turbulence closure models implemented using a generic length scale method. Ocean Modelling 8: 81-113.

Wang S, Yin K, Yuan P, Li H, Li S. 2010. Design and stability analyses of floating tidal current power generation test platform. In Power and Energy Engineering Conference (APPEEC), 2010 Asia-Pacific (pp. 1-4). IEEE.

Ward, SL, Neill, SP, Van Landeghem, KJJ and Scourse, JD. 2015. Classifying seabed sediment type using simulated tidal-induced bed shear stress. Marine Geology 367: 94-104

Winant CD, Gutiérrez de Velasco G. 2003. Tidal dynamics and residual circulation in a well-mixed inverse estuary. Journal of Physical Oceanography 33: 1365-1379.

Xie SP, Deser C, Vecchi GA, Collins M, Delworth TL, Hall A, Hawkins E, Johnson NC, Cassou C, Giannini A, Watanabe M. 2015. Towards predictive understanding of regional climate change. Nature Climate Change 5: 921.

Yang Z, Wang T, Copping A, Geerlofs S. 2014. Modeling of in-stream tidal energy development and its potential effects in Tacoma Narrows, Washington, USA. Ocean & coastal management 31: 52-62.

Yates N, Walkington I, Burrows R, Wolf J. 2013. Appraising the extractable tidal energy resource of the UK's western coastal waters. Phil. Trans. R. Soc. A. 28: 20120181.

Young EF, Aldridge JN, Brown J. 2000. Development and validation of a three-dimensional curvilinear model for the study of fluxes through the North Channel of the Irish Sea. Continental Shelf Research 20: 997-1035.

Figure 1

Click here to download high resolution image

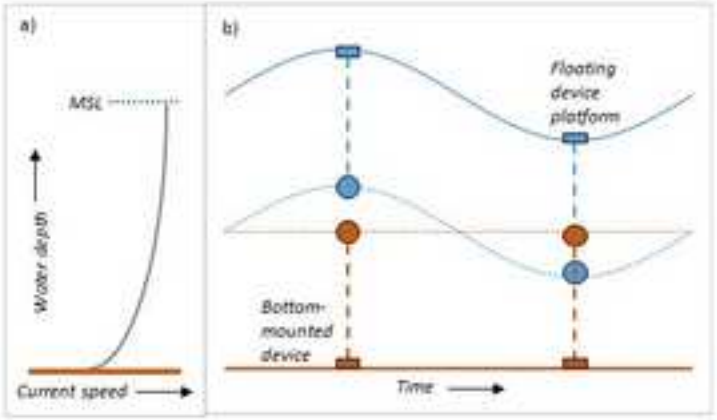

Figure 2

Click here to download high resolution image

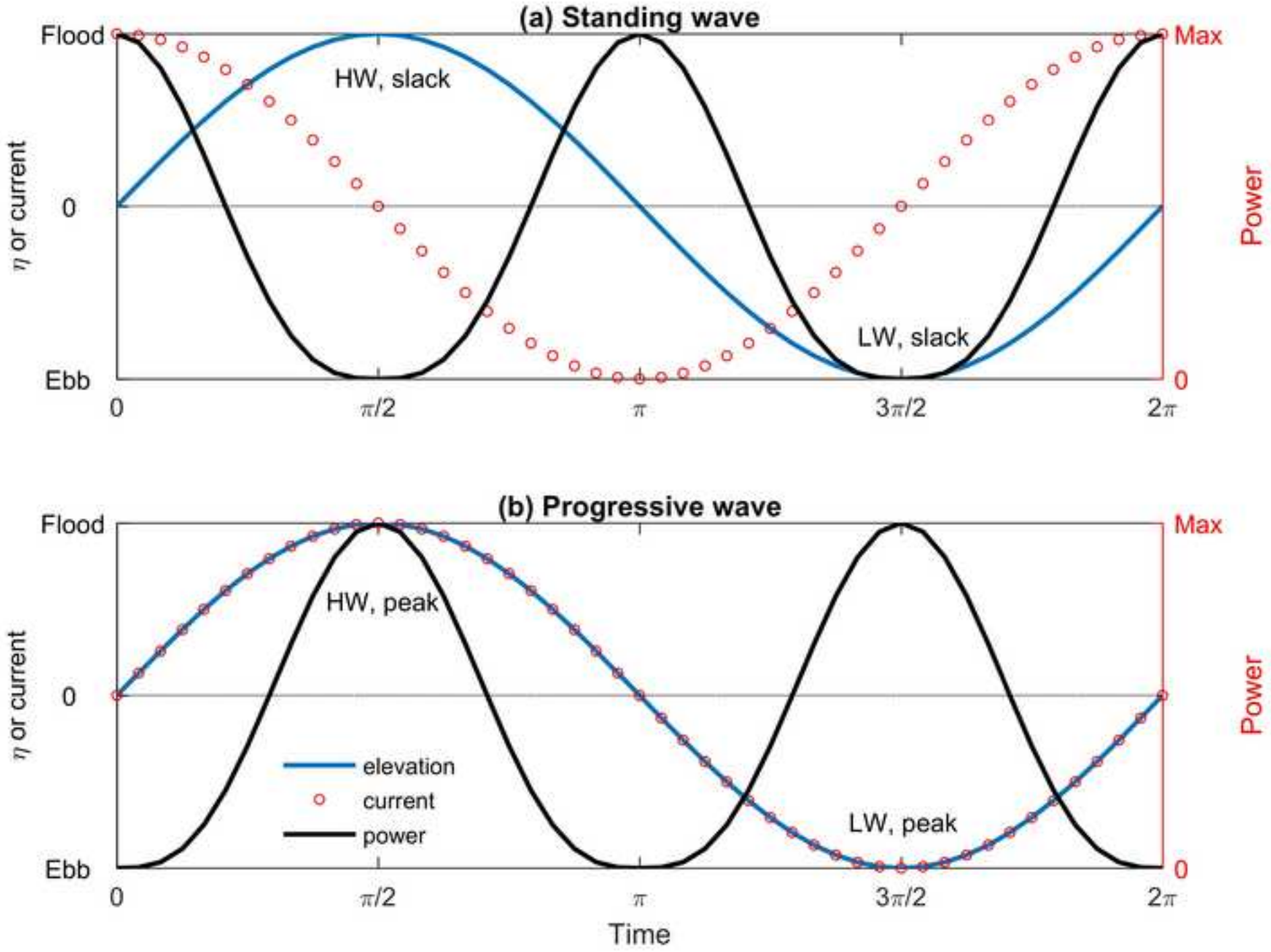

Figure 3

Click here to download high resolution image

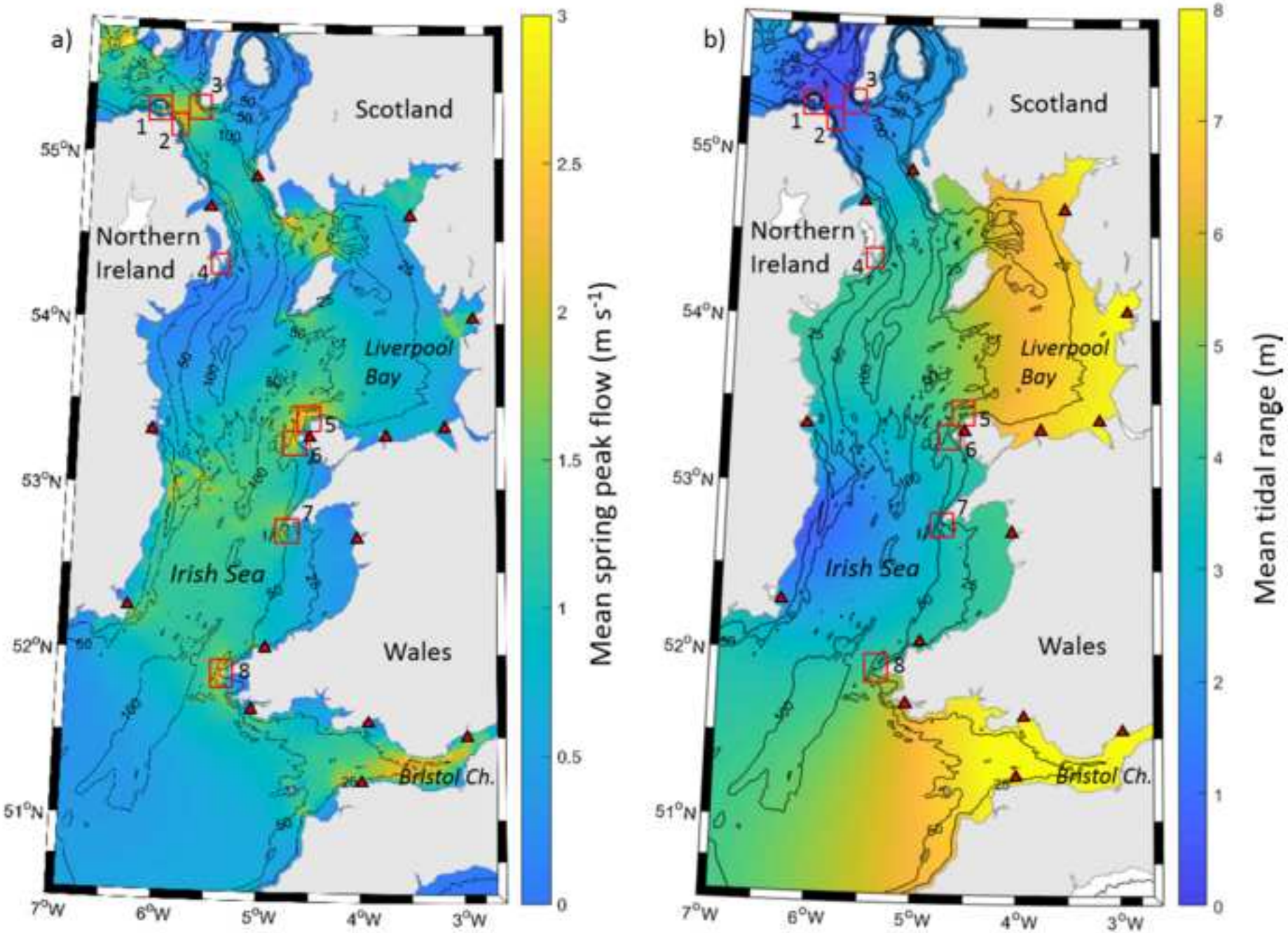

Figure 4

Click here to download high resolution image

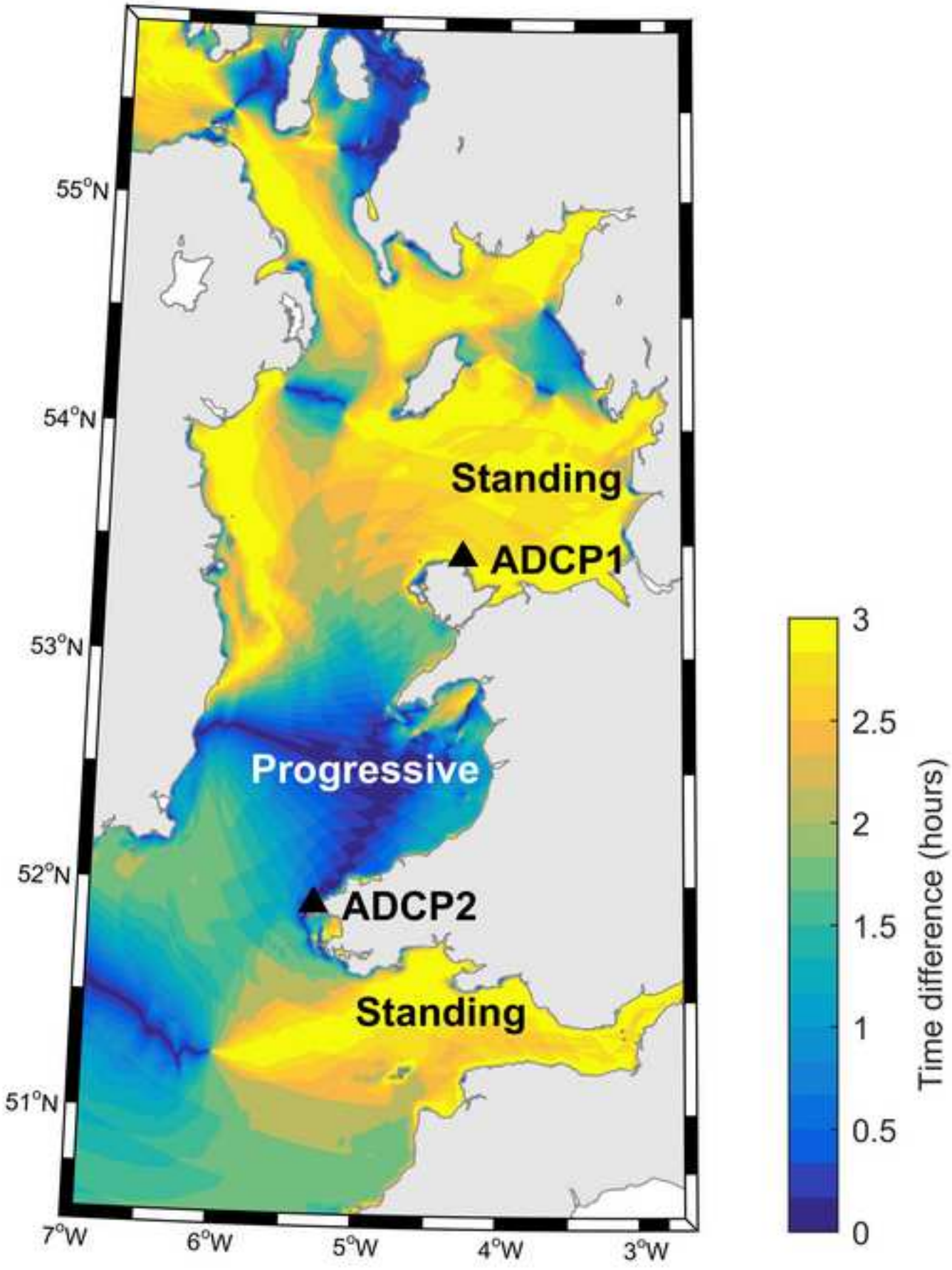

Figure 5

Click here to download high resolution image

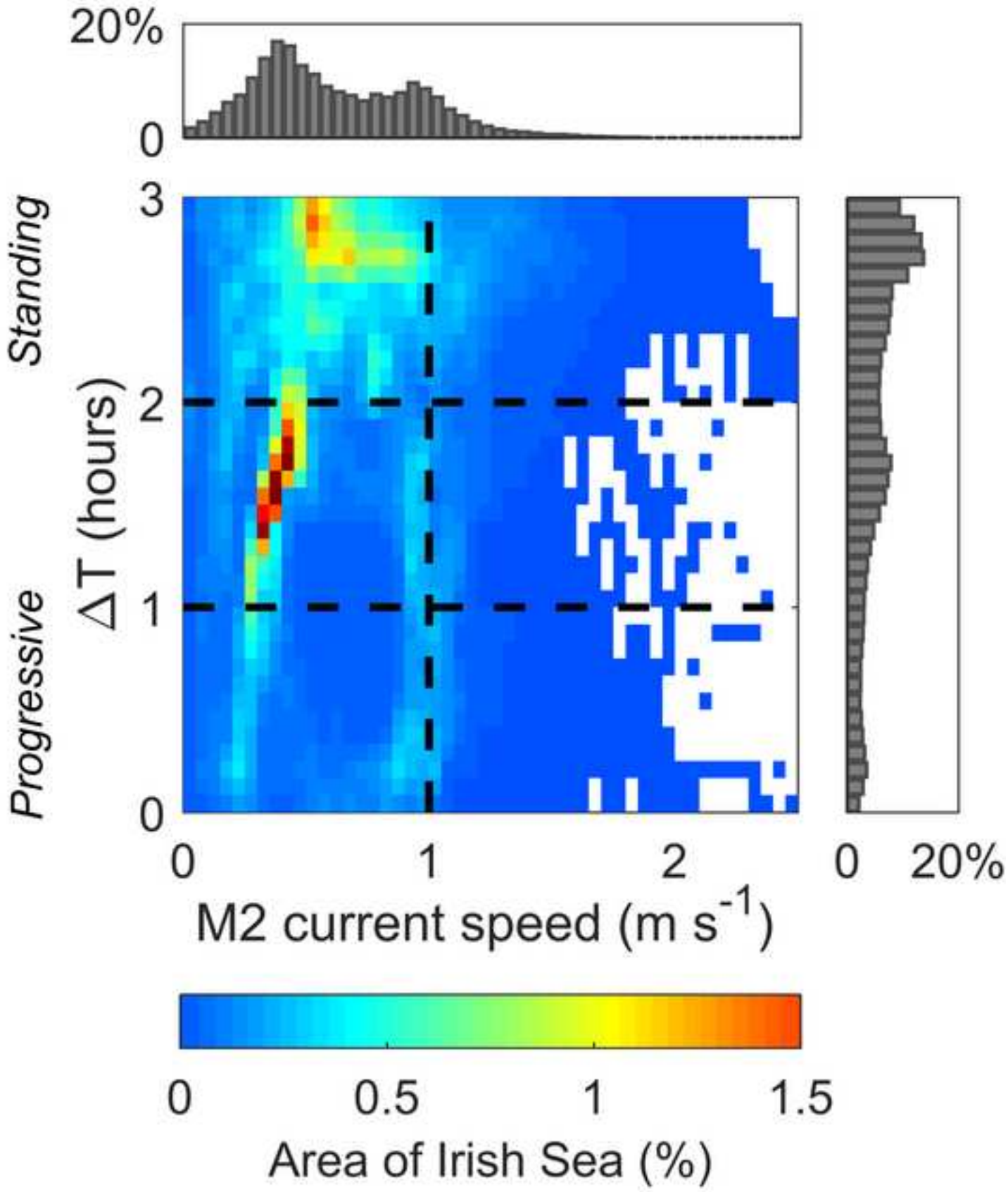

Figure 6

Click here to download high resolution image

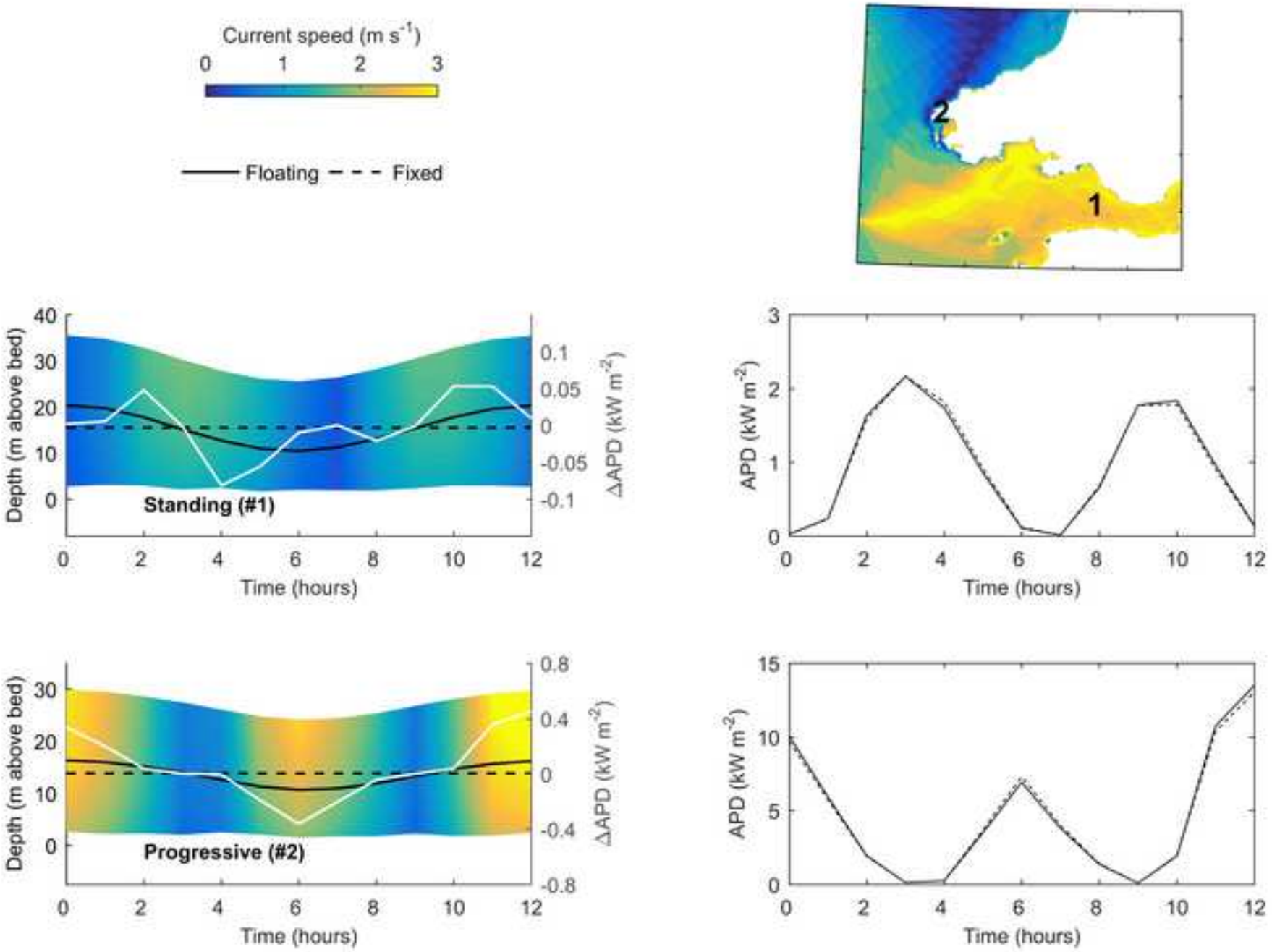

Figure 7

Click here to download high resolution image

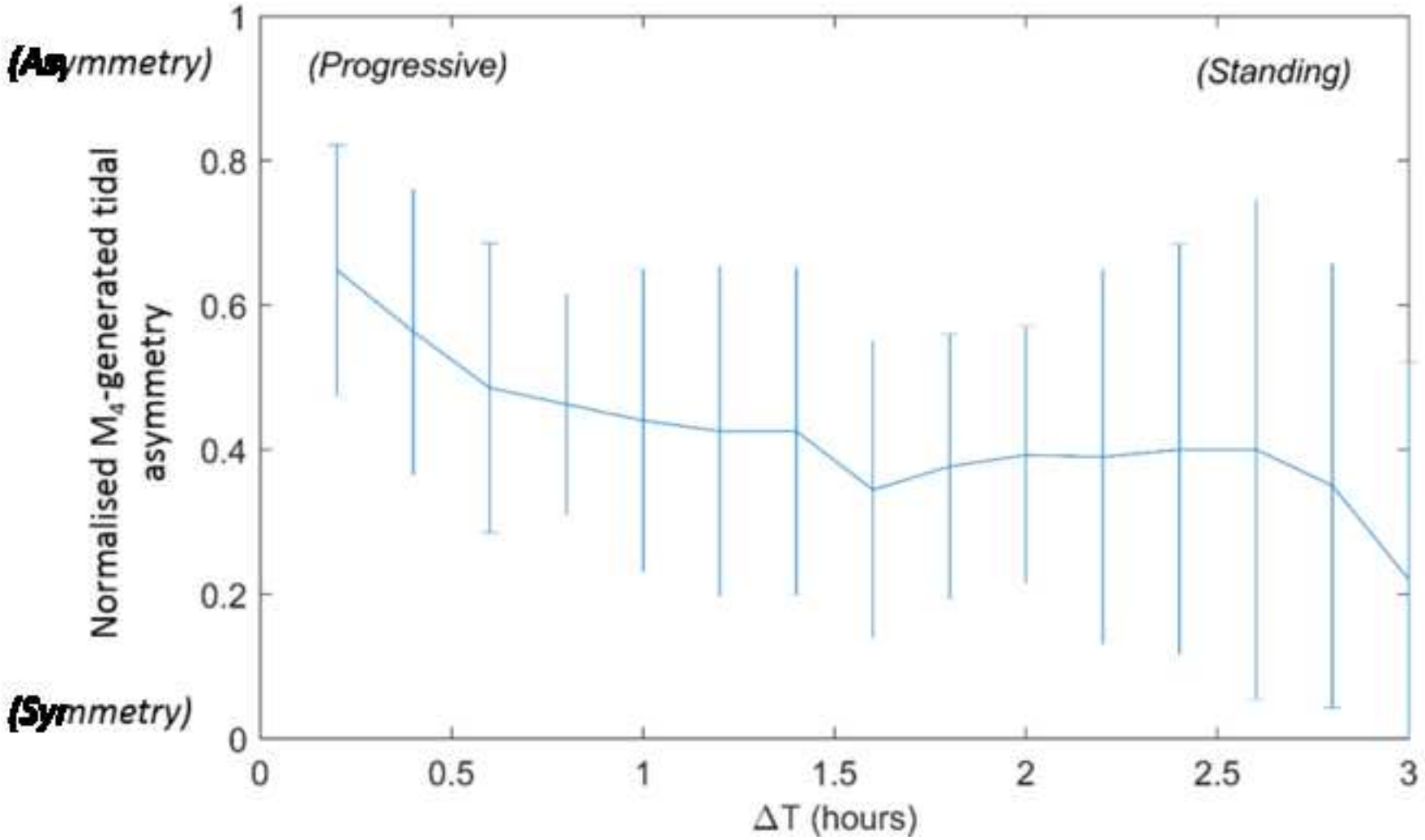

Figure 8 part 1

Click here to download high resolution image

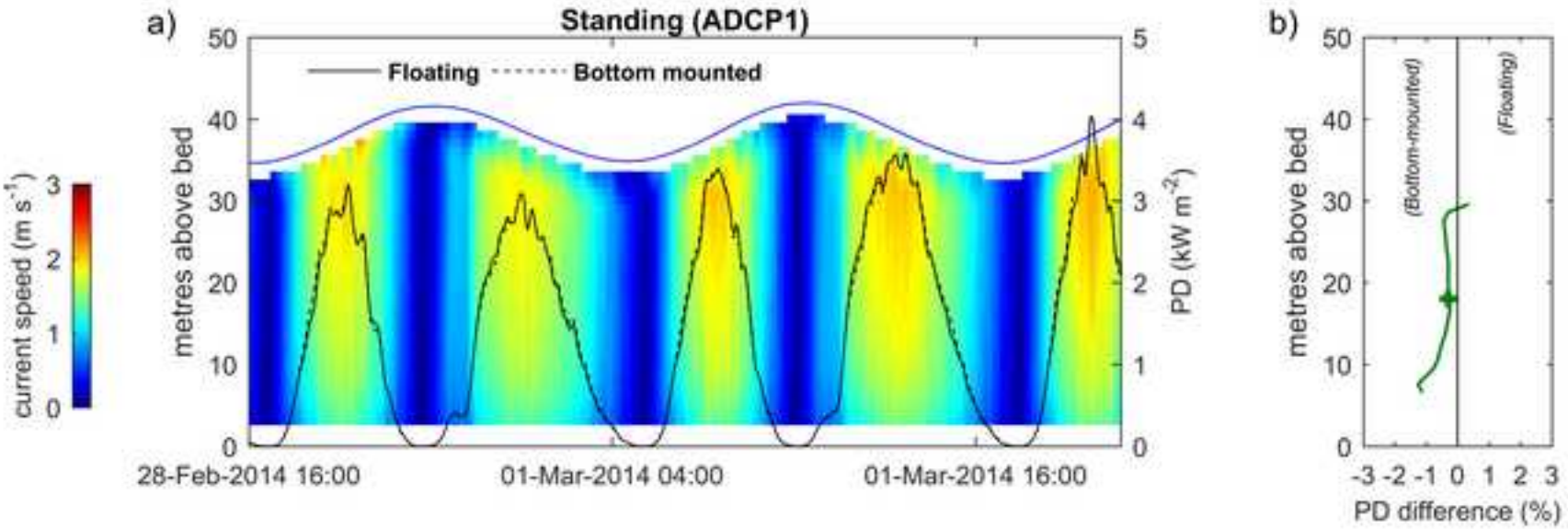

Figure 8 part 2

Click here to download high resolution image